Assembly and activation of dynein–dynactin by the cargo adaptor protein Hook3

Courtney M. Schroeder[1,2] and Ronald D. Vale[1,2]

[1]The Howard Hughes Medical Institute and [2]Department of Cellular and Molecular Pharmacology, University of California, San Francisco, San Francisco, CA 94158

Metazoan cytoplasmic dynein moves processively along microtubules with the aid of dynactin and an adaptor protein that joins dynein and dynactin into a stable ternary complex. Here, we examined how Hook3, a cargo adaptor involved in Golgi and endosome transport, forms a motile dynein–dynactin complex. We show that the conserved Hook domain interacts directly with the dynein light intermediate chain 1 (LIC1). By solving the crystal structure of the Hook domain and using structure-based mutagenesis, we identify two conserved surface residues that are each critical for LIC1 binding. Hook proteins with mutations in these residues fail to form a stable dynein–dynactin complex, revealing a crucial role for LIC1 in this interaction. We also identify a region of Hook3 specifically required for an allosteric activation of processive motility. Our work reveals the structural details of Hook3's interaction with dynein and offers insight into how cargo adaptors form processive dynein–dynactin motor complexes.

Introduction

Eukaryotic cells use molecular motors to transport and spatially organize organelles, proteins, and mRNAs within the cytoplasm. Cytoplasmic dynein is a molecular motor that carries cargo toward microtubule minus ends (Allan, 2011). Dynein is a large homodimer composed of two ~500-kD heavy chains that contain the ATPase motor domain (Schmidt, 2015; Bhabha et al., 2016). The N-terminal portion of the heavy chain binds additional subunits known as the dynein tail subunits, which include the light intermediate chain (LIC), intermediate chain (IC), and light chains (LCs; LC8, Tctex1, and LC7/roadblock; Pfister et al., 2006; Pfister and Lo, 2012). This tail complex is responsible for linking dynein to cargo (Pfister and Lo, 2012). Mammalian dynein is not constitutively active; rather, its motility is regulated by cargo interaction (McKenney et al., 2014; Schlager et al., 2014).

The mammalian LICs, encoded by two closely related gene products, LIC1 and LIC2 (Hughes et al., 1995; Tynan et al., 2000), are involved in several different types of cargo interactions and dynein-based movements, including endosomal and lysosomal transport, ER export, Golgi transport, and axonal vesicle trafficking (Koushika et al., 2004; Palmer et al., 2009; Horgan et al., 2010; Tan et al., 2011; Kong et al., 2013; Brown et al., 2014). The domain structure of the LIC allows it to interact with cargo adaptors while integrated into the dynein holoenzyme. The LIC's highly conserved N-terminal G protein–like domain binds directly to the dynein heavy chain, and the less conserved C-terminal domain binds adaptor proteins (Schroeder et al., 2014; Fig. 1 A). These cargo adaptors are themselves multifunctional proteins that can bind to a protein (e.g., a Rab GTPase) on a membranous cargo (Fu and Holzbaur, 2014; Cianfrocco et al., 2015; Carter et al., 2016).

In addition to binding dynein LIC and cargo, adaptor proteins promote an interaction between dynein and dynactin, a 12-subunit protein complex (Schroer, 2004). For mammalian dynein, the formation of this tripartite complex is important for long-distance movement (processivity) along microtubules (McKenney et al., 2014; Schlager et al., 2014). This mechanism has been best studied for Bicaudal D2 (BicD2), an adaptor that links dynein–dynactin to Rab6 on Golgi-derived vesicles (Dienstbier and Li, 2009). The N terminus of BicD2 consists of a 270-residue coiled coil that sits in a groove of the Arp1 filament of dynactin and also interacts with the N-terminal region of the dynein heavy chain; this dynein heavy chain-BicD2-Arp1 interaction was proposed to stabilize the tripartite complex (Urnavicius et al., 2015). The mechanism by which this interaction promotes motility is less clear. One possibility is that cargo adaptors activate an autoinhibited state of dynactin (McKenney et al., 2014), enabling it to bind to microtubules and initiating motility. Mammalian dynein also may be locked in an autoinhibited conformation (Torisawa et al., 2014), and cargo adaptors and dynactin may release this autoinhibited state and reposition the motor domains of the dynein dimers for motility (Urnavicius et al., 2015). These models, however, have not proposed a role for a LIC-adaptor protein interaction. Furthermore,

---

The Rockefeller University Press $30.00
J. Cell Biol. Vol. 214 No. 3   309–318
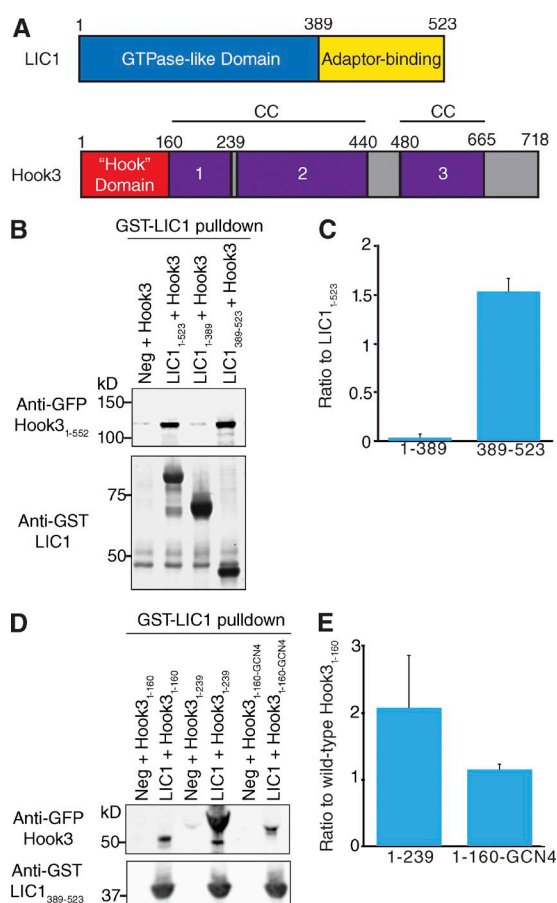www.jcb.org/cgi/doi/10.1083/jcb.201604002

JCB   309

Figure 1. **Dynein LIC binds the Hook domain.** (A) The domain architectures of human LIC1 and Hook3. See text for details. (B) GST-tagged human full-length or truncated LIC1 bound to glutathione resin were incubated with sfGFP-tagged Hook3$_{1-552}$, centrifuged and probed for Hook3 with an anti-GFP antibody. LIC1 in the pelleted beads was detected using an anti-GST antibody. Negative (Neg) control lacks LIC1 on the beads. (C) Ratio of band intensity to the full-length LIC1 signal in B; mean and SD from $n = 3$ independent experiments. (D) Two sfGFP-tagged Hook3 constructs were tested for LIC1 binding using the assay described in B. Also tested was a Hook domain artificially dimerized using a GCN4 sequence (Hook3$_{1-160-GCN4}$). (E) The ratio of band intensity to the Hook3$_{1-160}$ signal in B; mean and SD from $n = 3$ independent experiments.

it is unclear whether the assembly of the tripartite motor complex and activation of motility are separable functions.

One cargo adaptor that has been shown to assemble and activate dynein–dynactin is Hook3, although its mechanism has been less studied compared with BicD2. The Hook proteins, first identified for their role in endocytic cargo sorting in *Drosophila melanogaster* (Krämer and Phistry, 1999), are a widely expressed class of dynein-associated cargo adaptor proteins (Bielska et al., 2014; Zhang et al., 2014). *Drosophila* and fungi have a single Hook gene, whereas mammals have three Hook genes. The most conserved region of the Hook genes is found at the N-terminal domain (aa 1–160; Fig. 1 A). Without this Hook domain, Hook can no longer interact with dynein and dynactin (Bielska et al., 2014; Zhang et al., 2014). After the N-terminal domain are three coiled-coil domains that are important for dimerization (Krämer and Phistry, 1999; Walenta et al., 2001) and a divergent C-terminal domain that binds a variety of proteins specific for each Hook isoform (Walenta et al., 2001; Sano et al., 2007; Szebenyi et al., 2007; Moynihan et al., 2009;

Maldonado-Báez et al., 2013). All mammalian Hook isoforms form a complex with Fused Toes and the Fused Toes– and Hook-interacting protein; fungal homologs of these proteins are important for dynein-mediated early endosome transport by linking Hook to the cargo (Xu et al., 2008; Yao et al., 2014).

Here, we sought to understand the mechanism by which Hook3 interacts with dynein and dynactin and activates processive motility. We discuss the crystal structure of the Hook domain and show that this domain binds directly to the C-terminal region of LIC1. Structure-based mutagenesis studies revealed two conserved surface residues that are essential for this interaction. Abrogation of the LIC interaction renders Hook3 unable to join dynein and dynactin in a stable complex. Interestingly, although the N-terminal 239 residues of Hook3 are sufficient for forming a stable complex with dynein–dynactin, this tripartite complex is immotile; activation of motility requires a more distal coiled-coil region of Hook3. This result reveals that complex assembly and activation of motility are separable activities. Our data suggest a model for how Hook3 joins dynein and dynactin into a motile complex.

Results

The Hook domain of Hook3 binds to the dynein LIC

Hook3 is comprised of the N-terminal, highly conserved Hook domain (Walenta et al., 2001), followed by three coiled coils and a C-terminal cargo-binding region (Fig. 1 A). A yeast two-hybrid assay revealed an interaction between aa 1–236 of *Caenorhabditis elegans* Hook and the LIC (Malone et al., 2003). We sought to confirm a direct interaction between Hook3 and LIC1 using purified proteins, as we demonstrated previously for the adaptor proteins RILP, BicD2, and FIP3 (Schroeder et al., 2014). Previous work showed that Hook3$_{1-552}$ is sufficient to produce a highly processive dynein–dynactin–Hook3 complex (McKenney et al., 2014), and thus we used this slightly truncated Hook3 protein to test for interactions with LIC1. GFP-tagged Hook3$_{1-552}$ was incubated with beads coated with GST-tagged versions of either full-length LIC1, the LIC N-terminal G-domain (LIC1$_{1-389}$), or the C-terminal domain (LIC1$_{389-523}$); the beads and any interacting proteins were centrifuged, and the protein composition of the pull-down was analyzed by immunoblot. The results revealed that Hook3$_{1-552}$ cosedimented with full-length LIC1 and the LIC1 C terminus alone, but not with the N-terminal LIC1 G domain (Fig. 1, B and C; and Fig. S1 A). Thus, similar to the other cargo adaptors RILP, BicD2, and FIP3 (Schroeder et al., 2014), Hook3 also directly binds to LIC1$_{389-523}$.

We truncated Hook3$_{1-552}$ to identify a smaller fragment that might bind LIC1$_{389-523}$. The shorter truncation Hook3$_{1-239}$ bound to LIC1$_{389-523}$ in the pull-down assay (Fig. 1, D and E; and Fig. S1 B), and the two proteins co-eluted as a stable complex by gel filtration chromatography (Fig. S1 C). The Hook domain alone (Hook3$_{1-160}$) also bound LIC1$_{389-523}$, albeit more weakly than Hook3$_{1-239}$ (Fig. 1, D and E; and Fig. S1 B). Hook3$_{1-160}$ lacks the predicted coiled coil found in Hook3$_{1-239}$, and thus the stronger interaction of Hook3$_{1-239}$ might be because it is a dimer. We therefore tested an artificially dimerized coiled-coil version of Hook3$_{1-160}$ (Hook3$_{1-160-GCN4}$) but found that its binding affinity to LIC1 was not increased relative to the monomeric version (Fig. 1, D and E; and Fig. S1 B). Overall, these data
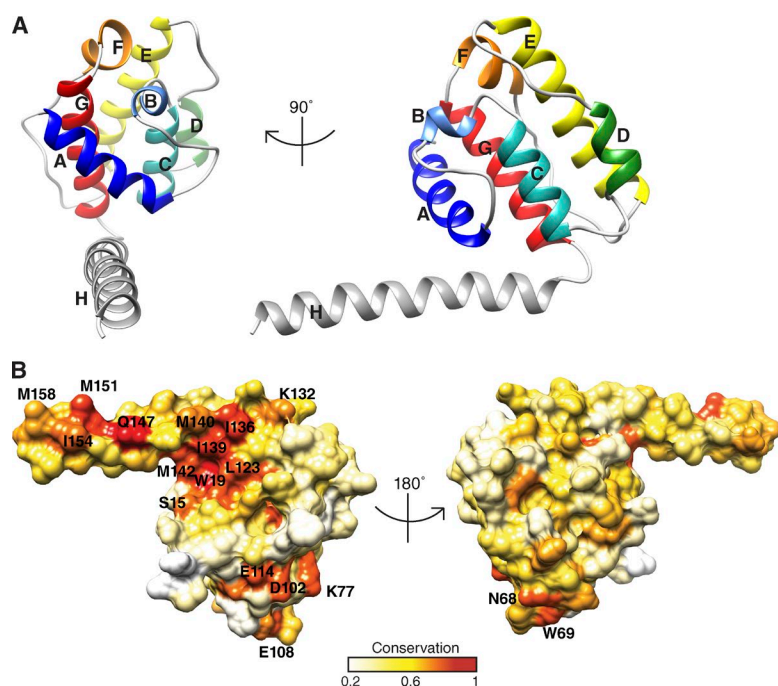
Figure 2. The structure of the Hook domain exhibits an extended α-helix and restricted conservation. (A) The 1.7-Å structure of the Hook domain (aa 9–158) from human Hook3 with the helices labeled A–H. Colors (helices A–G) denote the canonical CH domain. (B) The conservation of residues on the surface of the structure in A is shown with red representing the most conserved and white depicting the least conserved. Highly conserved residues are labeled.

indicate that the N-terminal Hook domain can bind specifically to the C-terminal region of LIC1 and that the region between aa 160 and 239 strengthens this interaction.

The Hook domain contains a calponin homology fold with an extended α-helix

We attempted to co-crystallize LIC1$_{389–523}$ with either Hook3$_{1–239}$ or Hook3$_{1–160}$, but crystals were obtained only for Hook3$_{1–160}$. A 1.7-Å dataset was obtained from one of the crystals, and a poly-alanine model based on a nuclear magnetic resonance (NMR) solution structure of mouse Hook1$_{1–160}$ (PDB 1WIX) was used for molecular replacement. After multiple rounds of refinement, the final structure has an R$_{work}$ of 18.4 and R$_{free}$ of 21.4 (Table 1). Two copies of the protein are present in the asymmetric unit and interact through an antiparallel arrangement of their C-terminal α-helices (helix H described later). This interaction may not be physiological because Hook3$_{1–160}$ is monomeric, as determined by static light scattering (unpublished data).

The Protein Homology/analogY Recognition Engine (PHYRE), which predicts a protein's tertiary structure based on homology, previously predicted that the Hook domain is comprised of a calponin homology (CH) fold (Zhang et al., 2014). Our structure indeed exhibits a canonical seven-helix CH fold (Fig. 2 A). However, the crystal structure reveals an additional eighth α-helix (helix H, aa 132–158; Fig. 2 A), which was not expected from prior secondary structure prediction (Drozdetskiy et al., 2015). This same α-helix also appears in the NMR structure of the Hook domain of mouse Hook1 (PDB 1WIX), but it is bent in the middle and folded back on itself (Fig. S2 A). Thus, it appears that helix H is able to adopt different conformations; the extended conformation that we have observed may be stabilized by protein–protein interactions in the asymmetric unit.

We next mapped the conserved surface residues in the Hook domain onto our crystal structure using an alignment of 19 Hook domain sequences ranging from fungal to mammalian species (Fig. S3). Strikingly, one side of the structure is much

more highly conserved than the other (Fig. 2 B). This contrast is even more evident in the map of conserved residues between the

Table 1. Crystallographic data and refinement statistics

Data collection	Data
Space group	P 2 2$_1$ 2$_1$
Cell dimensions	
a, b, c (Å)	33.92, 75.88, 111.85
α, β, γ (°)	90, 90, 90
Wavelength	1.11587
Resolution (Å)	45.0–1.7 (1.76–1.70)[a]
I/σI	15.36 (1.10)[a]
Completeness (%)	99.7 (99.8)[a]
Redundancy	7.0 (7.1)[a]
R$_{merge}$[b]	0.076 (1.952)[a]
CC$_{1/2}$	0.999 (0.498)[a]
Refinement	
Resolution (Å)	45.0–1.7 (1.76–1.70)[a]
Reflections, n	32,558 (3,178)[a]
R$_{work}$/R$_{free}$[c]	18.4/21.4 (30.3/33.1)[a]
No. nonhydrogen atoms	
Protein	2,426
Water	181
B-factors	
Protein	41.10
Water	46.30
Root mean square deviations	
Bond lengths (Å)	0.006
Bond angles (°)	0.91
Ramachandran favored (%)	98
Ramachandran outliers (%)	0
PDB code	5J8E

[a]Numbers in parentheses refer to the highest resolution shell.
[b]$R_{merge} = \sum_{hkl}\sum_i |I_{i(hkl)} - <I_{hkl}>| / \sum_{hkl}\sum_i I_{i(hkl)}$, where $I_{i(hkl)}$ is the scaled intensity of the ith measurement of a reflection and $<I_{hkl}>$ is the average intensity for that reflection.
[c]$R = \sum_{hkl} |F_{obs, hkl} - F_{calc,hkl}| / \sum_{hkl} |F_{obs,hkl}| \times 100$, where R_{free} was calculated on a test set comprising 4.2% of the data excluded from refinement.

three human Hook genes (Fig. S2, B and C). Several highly conserved residues lie within the extended helix H, including the universally conserved Q147 and nearby conserved hydrophobic residues. Two other prominent patches of conservation lie on this same face of the CH domain—one cluster consists mainly of hydrophobic residues (S15, W19, and L123), and the other consists of charged residues (K77, D102, E108, and E114).

Two highly conserved residues mediate the Hook3–dynein interaction and are critical for dynein–dynactin motility

The surface conserved residues could be part of a binding interface with the dynein light intermediate chain. To test which region of the Hook domain might be involved in binding LIC1, we made four proteins with different clusters of alanine mutations: (1) Q147A/M151A/I154A, (2) I136A/I139A/M142A, (3) N68A/W69A/K77A, and (4) D102A/E108A (Fig. 3 A). These mutations were made in the construct Hook3$_{1-239}$ because of its higher binding affinity to LIC1 than Hook3$_{1-160}$. The triple and double mutations produced monodisperse protein with a similar gel filtration pattern to the wild-type (WT) protein (Fig. S4 A). We tested each mutant Hook3 protein for binding to GST-LIC1$_{389-523}$ using the bead pull-down assay (Fig. 3, B and C; and Fig. S4 B). The triple mutants Q147A/M151A/I154A and I136A/I139A/M142A exhibited little or no detectable binding. In contrast, the triple mutant N68A/W69A/K77A and the double mutant D102A/E108A showed little difference in binding (Fig. 3, B and C; and Fig. S4 B). Because patches Q147A/M151A/I154A and I136A/I139A/M142A both lie within helix H, these results suggest that the highly conserved helix H contains the main LIC1 binding interface.

We investigated the more solvent-exposed Q147A/M151A/I154A patch in more depth with single-point mutants. The gel filtration of the Q147A, M151A, and I154A mutants also show monodisperse protein, as shown with the triple mutants (Fig. S4 A). Strikingly, the single I154A and Q147A mutations each led to a dramatic reduction in the Hook3–LIC1 interaction (Fig. 4, A and B; and Fig. S4 C). In contrast, the Hook3 mutant M151A could still bind LIC1 as well as WT (Fig. 4, A and B; and Fig. S4 C).

We tested whether these single-point mutants affected the binding of Hook3$_{1-552}$ to intact dynein and dynactin in a porcine brain lysate (McKenney et al., 2014). WT Hook3$_{1-552}$ pulled down dynein–dynactin as previously reported (McKenney et al., 2014), but no detectable endogenous BicD2 (another cargo adapter that can bind dynein–dynactin; Fig. S4, D and E). In contrast, the Hook3 single-point mutants Q147A and I154A bound very little or no dynein and no detectable dynactin, whereas the M151A mutant bound dynein–dynactin in a manner similar to WT (Fig. 4, C and D; and Fig. S4 E). These results indicate that the highly conserved residues Q147 and I154 in helix H of Hook3 both play critical roles in binding LIC1 and forming a stable dynein–dynactin complex.

We next investigated the ability of Hook3 mutant proteins to stimulate dynein–dynactin motility (McKenney et al., 2014). Dynein and dynactin, purified from a human RPE-1 cell line (Fig. S4 F), were preincubated with GFP-tagged Hook3 constructs. The mixture was then added in the presence of ATP to glass-immobilized microtubules, and interactions of GFP-Hook3 with microtubules were examined by total internal reflection fluorescence (TIRF) microscopy. Processive movement of dynein–dynactin and WT GFP-Hook3 was observed as
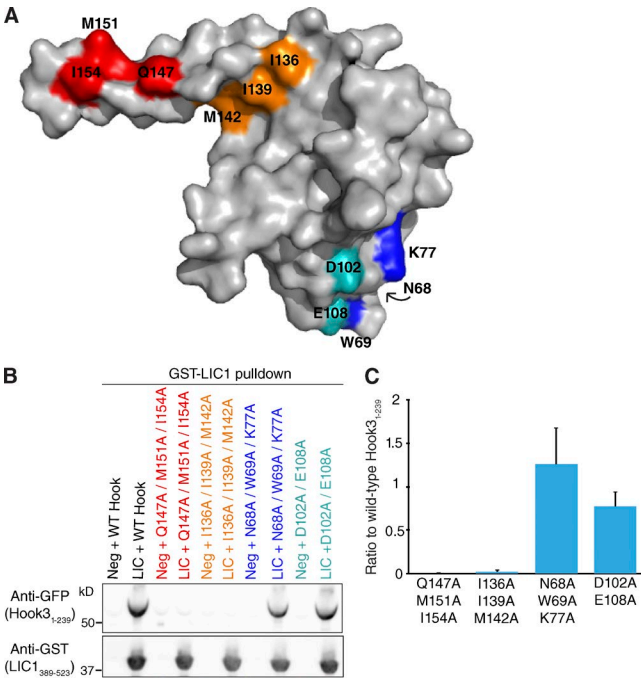
previously described (McKenney et al., 2014). The point mutant M151A produced a similar number of motile dynein–dynactin–Hook3 molecules compared with WT GFP-Hook3 (Fig. 4, E and F), and the velocities of the molecules were in a similar range as WT Hook3 (Fig. S5 C). In contrast, Q147A and I154A GFP-Hook3 constructs did not elicit processive runs (Fig. 4, E and F), presumably because they did not bind to and form a complex with dynein and dynactin. Thus, Q147 and I154 are each essential for Hook3's interaction with LIC1 and for the formation of a processive dynein–dynactin complex.

Hook3 truncations that assemble dynein–dynactin do not elicit processive motility

We sought to define the roles that the Hook domain and the extended coiled coil domains of Hook3 play in assembling dynein and dynactin into a complex. Previous work on the 270-residue coiled-coil domain of BicD2 showed that it sits in the groove of the dynactin Arp1 filament and creates a binding interface with the dynein heavy chain (Urnavicius et al., 2015). We made two constructs that consisted primarily of the Hook domain (aa 1–160 and 1–239), truncations that excluded the Hook domain (aa 160–552 and 239–552), and a truncation that excluded just the CH domain but contained helix H of the Hook domain (aa 130–552; Fig. 1 A). These constructs, bound to Strep-Tactin resin, were incubated with porcine brain lysate and then assessed for their ability to pull down the endogenous dynein–dynactin complex by immunoblotting for the dynein IC and the dynactin subunit p150. The construct Hook3$_{1-239}$ pulled

Figure 3. **Helix H in the Hook domain contains a LIC-binding interface.** (A) Patches of conserved residues in the Hook domain were mutated in separate constructs. Each patch of residues is denoted by a different color. (B) GST-LIC1$_{389-523}$, bound to glutathione resin, was incubated with sfGFP-Hook3$_{1-239}$ mutants. The beads were centrifuged, and then Hook3 binding was assessed by immunoblot analysis using an anti-GFP antibody. The presence of the bait GST-LIC1$_{389-523}$ was verified using an anti-GST antibody. Negative control lacks LIC1 on the beads. (C) Ratio of band intensity to the WT Hook3$_{1-239}$ signal in B; mean and SD from $n = 3$ independent experiments.

Hook3$_{1-160}$ and Hook3$_{1-239}$ are analogous to the relative binding affinities for purified LIC1 (Fig. 1, D and E). The constructs lacking the Hook domain did not pull down dynein or dynactin, similar to what was found in vivo for HookA in *Aspergillus nidulans (*Zhang et al., 2014). Overall, these data demonstrate the importance of the Hook domain for the formation of this tripartite motor complex.

Because Hook3$_{1-239}$ did not bind as much dynactin as Hook3$_{1-552}$, we next investigated dynein–dynactin binding with a series of Hook3 truncations ending at residues 310, 348, 402, or 440 (residues chosen based on the low probability of perturbing the structure of coiled coil 2; Lupas et al., 1991; Fig. S5 B). Lengthening the coiled-coil domain from residue 239 to 552 did not significantly change the amount of dynein that was pulled down with Hook3 from the brain lysate (Fig. 5, C and D; and Fig. S5 A). However, lengthening the coiled coil resulted in a progressive increase in the amount of interacting dynactin (Fig. 5, C and D; and Fig. S5 A). These results suggest that it is not essential for the Hook3–dynein–LIC1 interaction. However, a longer Hook3 coiled coil is able to increase the affinity of dynein–Hook3 for dynactin.

We tested the microtubule binding ability and motility of the dynein–dynactin complex with Hook3$_{1-239}$, Hook3$_{1-402}$, Hook3$_{1-440}$, and Hook3$_{1-552}$. In this experiment, dynein and dynactin were first purified by affinity chromatography (see Methods) and then incubated with these truncated Hook proteins. Surprisingly, in the presence of ATP and dynein–dynactin, all of the truncations induced poor single-molecule motility compared with Hook3$_{1-552}$ (Fig. 5, E and F). Hook3$_{1-239}$ produced no processive motility at all, and even the longer constructs Hook3$_{1-402}$ and Hook3$_{1-440}$ produced very few motile events (Fig. 5, E and F). The few complexes that were motile with Hook3$_{1-402}$ and Hook3$_{1-440}$ exhibited similar velocities to Hook3$_{1-552}$ (Fig. S5 C). We tested whether the smallest truncation Hook3$_{1-239}$ might be unstable after addition of ATP, but found only a slight (18%) dissociation of dynein from the tripartite complex on beads after a 1-h incubation with 2.5 mM ATP (Fig. S5, D–F). In the microscopy assay in the absence of ATP, all Hook3 truncations did not bind microtubules alone (Fig. S5 G), but bound statically to microtubules in the presence of dynein–dynactin (Fig. 5, G and H). The results suggest that dynein–dynactin complexed with short Hook3 constructs can bind to microtubules in the absence of ATP (rigor microtubule binding with a low dissociation rate) but do not engage in a productive motility cycle in the presence of ATP (see Discussion). These findings indicate that the region of the coiled coil between aa 402 and 552 of Hook3 is required for robust activation of motility of the dynein–dynactin–Hook3 complex.

Discussion

In this study, we delineated the minimal binding regions for Hook3 that are required for two activities: (1) binding to the LIC1 C-terminal domain (Hook3$_{1-160}$) and (2) producing a dynein–dynactin complex that engages in robust processive motility (Hook3$_{1-552}$). Together, these results suggest a model for how cargo adaptors might regulate the minus end–directed motility of dynein–dynactin.

Our work provides structural insights into how Hook3 binds to dynein. We previously found that the C-terminal half of LIC1 is the docking site for several cargo adaptors (Schroeder
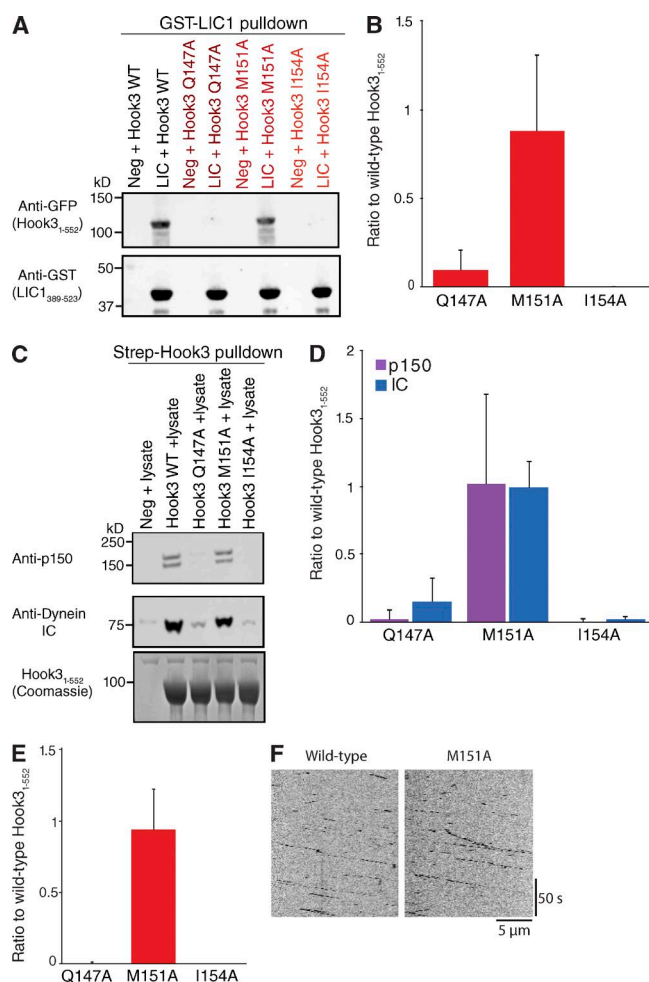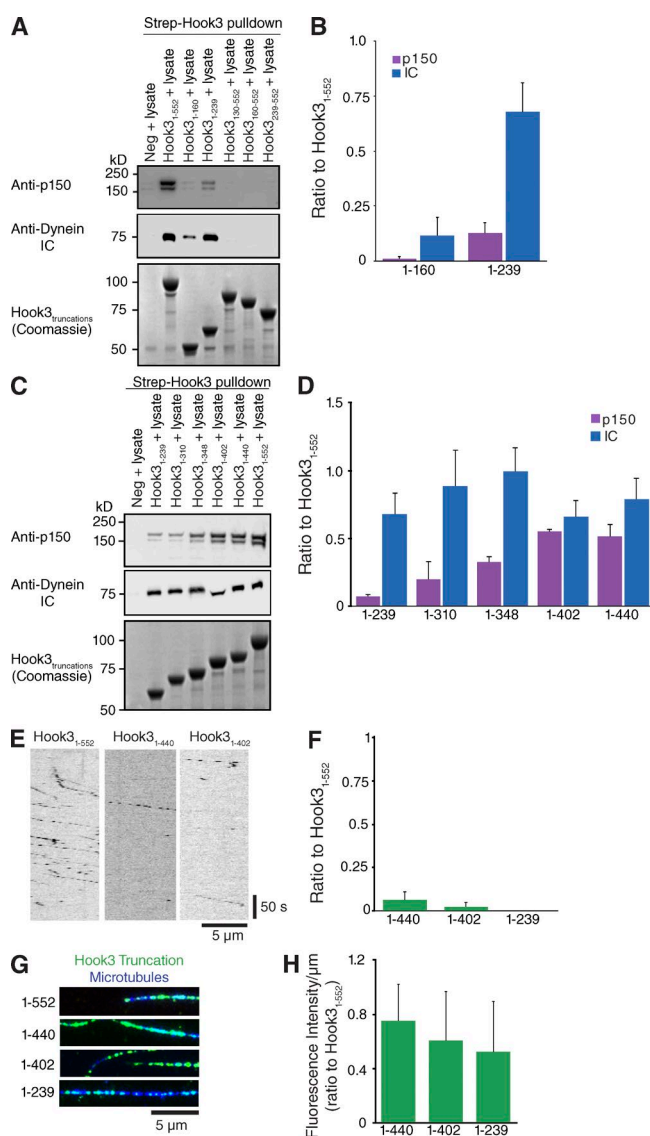

Figure 4. **Two conserved Hook3 residues are critical for the assembly and motility of dynein–dynactin.** (A) Single-point mutations Q147A, M151A, and I154A in sfGFP-tagged Hook3$_{1-552}$ were compared with WT and tested for binding to human GST-LIC1$_{389-523}$ as in Fig. 3 B (representative of triplicate experiments). Negative control lacks LIC1 on the beads. (B) Ratio of band intensity to the WT Hook3$_{1-552}$ signal in A; mean and SD from n = 3 independent experiments. (C) StrepII-Hook3 constructs, bound to Strep-Tactin resin, were incubated with porcine brain lysate; the beads were centrifuged; and the resin analyzed by immunoblotting for the dynein intermediate chain (IC) and the p150 subunit of dynactin. Negative control lacks Hook3 on the beads. The amount of each Hook3 construct was assessed by Coomassie stain. (D) Ratio of band intensity to the WT Hook3$_{1-552}$ signal in C; mean and SD from n = 3 independent experiments. (E) WT and single-point mutants were incubated with affinity-purified human dynein–dynactin and 1 mM ATP. SfGFP-tagged Hook3$_{1-552}$ was visualized by TIRF microscopy and classified as processive if it moved unidirectionally for >1 µm along microtubules. All constructs were normalized by dividing the total number of processive motors by the total length of microtubules in the field of view and the time of the movie (movements/µm per min). The ratios of the mutants to WT were calculated from side-by-side experiments performed on the same day. Shown are the mean ± SD of the ratios from three independent experiments performed on different days. The mean number of motile WT Hook3 molecules/µm per min was 0.039 ± 0.016. (F) Representative kymographs are shown for each construct that displayed motility. The kymographs are displayed using the same brightness and contrast.

down both dynein and dynactin, albeit to a lesser extent than the longer Hook3$_{1-552}$ (Fig. 5, A and B; and Fig. S5 A). Hook3$_{1-160}$ pulled down a small amount of dynein, but the dynactin signal was similar to that of the negative control (Fig. 5, A and B; and Fig. S5 A). The relative amounts of dynein pulled down by

Figure 5. **Hook3 truncations that bind dynein–dynactin are not sufficient for motility.** (A) Truncations of strepII-Hook3 were tested for binding to endogenous dynein–dynactin in porcine brain lysate as in Fig. 4 C. (B) The ratio of band intensity to the WT Hook3$_{1-552}$ signal in A; mean and SD from n = 3 independent experiments. The truncations not shown were measured to be the same as or less than the signal of the negative control. (C) C-terminal strepII-Hook3 truncations were tested for binding porcine brain dynein–dynactin as in A. The intermediate chain (IC) band in the lane for Hook3$_{1-402}$ is skewed because the IC and this Hook truncation run at the same molecular weight. (D) The ratio of band intensity to the WT Hook3$_{1-552}$ signal in C; mean and SD from n = 3 independent experiments. The following p-values are given for the truncations that differ statistically from Hook3$_{1-552}$: dynactin signal–Hook3$_{1-239}$, P < 0.0001; Hook3$_{1-310}$, P < 0.001; Hook3$_{1-348}$, P < 0.0001; Hook3$_{1-402}$, P < 0.0001; Hook3$_{1-440}$, P < 0.001; IC signal–Hook3$_{1-239}$, P = 0.03; and *Hook3$_{1-402}$, P < 0.05; *, The IC signal is disrupted by the similar size of Hook3$_{1-402}$. (E) Hook3 constructs were tested for their ability to activate motility of the dynein–dynactin complex in the presence of ATP (see Fig. 4 E). Representative kymographs are shown for each construct that moved. The kymographs are displayed using the same brightness and contrast. (F) Ratios of the motile shorter constructs to Hook3$_{1-552}$ were calculated from side-by-side experiments performed on the same day. Shown are the mean and SD of the ratios from three independent experiments performed on different days. The mean number of motile Hook3$_{1-552}$ molecules/µm per min was 0.070 ± 0.060. (G) The indicated truncations of sfGFP-Hook3 were incubated with affinity-purified human dynein–dynactin, and fluorescence binding to surface-immobilized microtubules was assessed in the absence of

et al., 2014), and we show here that Hook3 binds to this same region of the LIC. Helix H of Hook3, which extends from the CH domain, plays a key role in the LIC interaction, and our structure–function studies reveal two patches of residues in helix H (I136/I139/M142 and Q147/I154) that are involved in the interaction. These residues are highly conserved among all Hook isoforms, and thus it is likely that all Hook gene products bind LIC with a similar mechanism. Interestingly, residue I154 in human Hook3, which we find plays a key role in the LIC interaction, corresponds to L150 in *Aspergillus nidulans*, which is part of the *A. nidulans* double mutant (L150P/E151K) shown to disrupt early endosome transport and the HookA–dynein–dynactin interaction in vivo (Zhang et al., 2014). Our work corroborates this in vivo finding and provides structural insight into I154's conserved role in binding dynein.

The two residues (I154 and Q147A) that we have identified in Hook as being critical for the LIC interaction are located on one face of a helix (helix H) that extends from the CH domain. Mutations of these residues to alanine do not appear to affect protein stability, because these mutant proteins are not aggregated and behave similarly to the WT protein on gel filtration. The alanine mutants may reduce the affinity for the LIC by reducing the binding energy of the protein–protein interaction. Alternatively, the mutations could affect a conformational state of this helix. Interestingly, in the unpublished NMR structure of the mouse Hook1 domain (PDB 1WIX), helix H is bent, and the residues described earlier are sequestered in the middle of this bent conformation of helix H. Thus, based on these two Hook domain structures, we speculate that helix H may be capable of undergoing a conformational change that could regulate its interaction with the dynein LIC. Mutations in helix H might affect this conformational equilibrium. In addition, Hook3$_{1-239}$ may be able to bind LIC1 better than Hook3$_{1-160}$ because this longer construct might shift a conformational equilibrium of helix H toward its extended form. To test these ideas, further work will be needed to measure the conformational state of this helix.

Although the minimal Hook domain aa 1–160 binds the dynein LIC, it does not appear to be sufficient to recruit the dynactin complex. The first coiled coil of Hook3 (aa 160–239) enables dynactin binding, and the additional coiled coil sequence further enhances this interaction. A cryo-EM study revealed that the 270-residue coiled coil of another cargo adaptor, BicD2, interacts along the groove of the Arp1 filament of dynactin and also mediates an interaction with the dynein heavy chain (Urnavicius et al., 2015). Similar to BicD2, Hook3's coiled coils may sit in the groove of the Arp1 dynactin filament and promote an interaction between dynein and dynactin. Hook3$_{1-440}$, for example, may have ∼270 residues of coiled coil. However, the coiled coil of Hook3 (aa 160–552) alone is insufficient for stabilizing the tripartite complex, indicating that the Hook3–LIC1 interaction is also required. Supporting this conclusion, single-point mutations in Hook3 (either Q147A or I154A) that abrogate LIC1 binding also completely block the ability of Hook3 to form a

ATP; overlay shows Hook3 in green and microtubules in blue (images are displayed using the same brightness and contrast). (H) The fluorescence quantification for each condition is shown (mean fluorescence intensity [arbitrary units] of Hook3 per micrometer of microtubule). For each condition, >30 microtubules were quantified, and three replicate experiments were performed on different days (mean and SD, with the SD representing the variation in the ratio of intensity per micrometer).

dynein–dynactin complex. Thus, multiple protein–protein interfaces of the adaptor Hook3 with the dynein heavy chain, LIC1, and dynactin appear to be required to form a stable tripartite motor complex.

We also show that the C-terminal region of our Hook3 construct is required for robust activation of dynein motility. several possible models could explain how this additional coiled coil–containing region converts an inactive dynein–dynactin–adaptor complex (e.g., one formed by Hook3$_{1-239}$) into an active processive motor (one formed by Hook3$_{1-552}$; Fig. 6). First, a certain length of Hook3 bound along the dynactin Arp1 filament may be required to induce an allosteric conformational change in the dynein heavy chains to release them from an inhibited state (Chowdhury et al., 2015; Urnavicius et al., 2015). For example, an autoinhibited state of dynein may exist in which the two motor domains are stacked, necessitating the separation and alignment in the same direction to become active (Torisawa et al., 2014). An alternative and not mutually exclusive model involves the allosteric regulation by Hook3 of the N-terminal CAP-Gly domain of dynactin's p150 subunit. The p150 subunit regulates dynein motility (Kardon et al., 2009; McKenney et al., 2014; Tripathy et al., 2014), and p150's CAP-Gly domain binds to the C terminus of tubulin, an interaction that greatly enhances an initial microtubule binding encounter of dynein–dynactin–BicD2 that leads to processive movements (McKenney et al., 2016). However, dynactin alone exhibits minimal binding to microtubules, suggesting that it is in an autoinhibited state (Kardon et al., 2009; McKenney et al., 2014). This finding agrees with a dynactin cryo-EM structure showing that the junction between CC1A and CC1B in p150 is positioned near the pointed end of the Arp1 filament; in this folded conformation, the CAP-Gly and CC1A domains are unlikely to be accessible to the microtubule (Urnavicius et al., 2015). In a lower-resolution structure of the dynein–dynactin–BicD2 complex, the C terminus of a 270-aa coiled coil of BicD2 is located at the pointed end of the dynactin Arp1 filament (Urnavicius et al., 2015). We speculate that the C-terminal end of our motility-inducing Hook3 construct (aa 400–552) may somehow act to dislodge CC1A-CC1B from the backbone of the Arp1 filament. The release of p150 may enable this subunit to extend fully into an active conformation, enabling access to the microtubule (Fig. 6).

Although our data reveal an important role of the LIC in Hook3-mediated dynein motility, several questions remain unanswered. First, it is unknown whether the LIC acts as a passive tether for linking the motor domain to cargo adaptors or whether it also undergoes a conformational change that plays an active role in eliciting dynein motility. Second, it remains to be determined whether other cargo adaptors that interact with LIC1 (e.g., FIP3, RILP, and BicD2) do so through mechanisms similar to or different from those of Hook proteins. Among these adaptors, the Hook domain appears to be unique. Third, we also do not know how many cargo adaptors interact with dynein chains other than the LIC. For example, BicD2 has been shown to interact with both the dynein intermediate chain (Hoogenraad et al., 2001, 2003) and the light intermediate chain (Schroeder et al., 2014). Differences in activation among the adaptors might allow for many ways of regulating dynein-based cargo transport. Many of these important questions can be addressed through structural and functional studies of multiple types of cargo adaptor proteins interacting with dynein and dynactin.
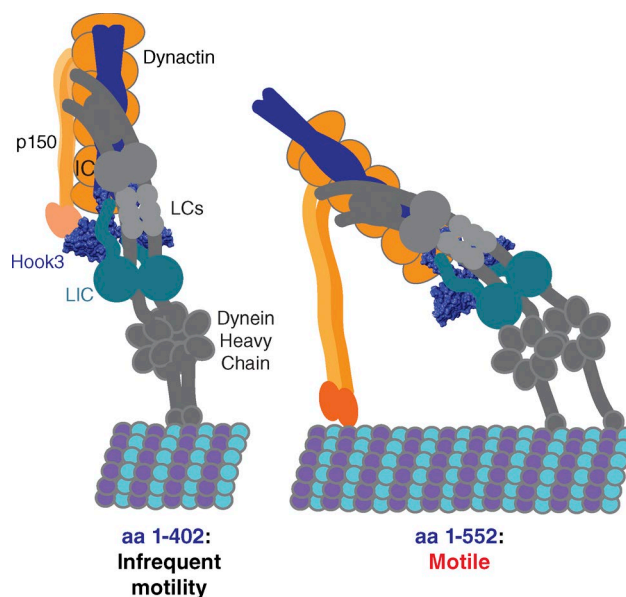

Figure 6. **Model of assembly and activation of the dynein–dynactin–Hook3 complex.** Short Hook constructs (e.g., Hook3$_{1-402}$) are able to assemble the tripartite motor complex by binding the LIC1 C-terminal domain and part of the dynactin Arp1 filament and dynein heavy chain. However, the complex is inactive for motility. We speculate that the longer coiled coil of Hook3$_{1-552}$ releases the CAP-Gly domain of p150 from an autoinhibited state to enable its binding to microtubules, thus enhancing the initiation of processive motility. A change in the orientation or other allosteric change in the motor domains, based on the work of Urnavicius et al. (2015) and Torisawa et al. (2014), also might be promoted by the longer Hook3 constructs. The illustration of the dynein–dynactin complex is based on work by Urnavicius et al. (2015) and Chowdhury et al. (2015). The length of Hook3$_{1-402}$, which contains ~240 residues of coiled coil, is estimated based on the dynein–dynactin–BicD2 cryo-EM structure (Urnavicius et al., 2015), which contained a 270-residue coiled coil. The illustration of the Hook3$_{1-552}$ coiled coil was then made proportional to the length of Hook3$_{1-402}$ based on the ratio of residues.

Materials and methods

Molecular biology

The cDNA of Hook3 was obtained from a human cDNA library made from mitotic RPE-1 cells, and all Hook3 constructs were cloned into vector pET28a with an N-terminal 6× His-strepII-superfolder GFP (sfGFP) tag. All human LIC1 (RefSeq accession number NM_016141.3) constructs were cloned into pGEX6P1, which included an N-terminal GST tag and a C-terminal strepII tag. Truncations were based on both secondary structure prediction (Drozdetskiy et al., 2015) and coiled coils prediction (Lupas et al., 1991). To dimerize the Hook3$_{1-160}$ construct, the GCN4 sequence (Harbury et al., 1993) was added to the C terminus. The 29-aa sequence was VKQLEDKVEELLSKNAHLENEVARLKKLV. Full-length human FIP3 (GenBank accession number AB383948) was cloned into pET28a with a strepII-SNAP tag and was used for the purification of the dynein–dynactin complex from porcine brain lysate.

Protein purification

All human Hook3 constructs were transformed into the *Escherichia coli* strain BL21 RIPL, and expression was induced with 0.5 mM IPTG at 37°C for 3–6 h. Bacterial pellets were resuspended with lysis buffer (25 mM Hepes, pH 7.8, 150 mM NaCl, 2 mM TCEP, 1 mM PMSF, and a protease inhibitor cocktail [Roche], 1 tablet per 50 ml) and lysed using an Emulsiflex press (Avestin). The lysate was clarified by centrifugation at 40,000 *g* for 30 min, and Hook3 was purified using Strep-Tactin

Superflow Plus resin (QIAGEN). The agarose was then washed with lysis buffer (excluding the Roche protease inhibitor cocktail) at ~20× the resin volume, and the purified protein was eluted with 3 mM desthiobiotin. The protein was concentrated and flash frozen. Thawed protein was then further purified by gel filtration with a Superose 6 10/300 GL or a Superdex 200 10/300 GL column (GE Healthcare). The gel filtration buffer was 30 mM Hepes, pH 7.8, 150 mM NaCl, 2 mM MgCl$_2$, 5% glycerol, and 2 mM TCEP. The Hook3-containing fractions were pooled, concentrated, and flash frozen. StrepII-SNAP-FIP3 was purified the same way as Hook3, except the lysis buffer included 25 mM Tris, pH 8.5.

GST-LIC1-strepII constructs (full length and truncations) were expressed as performed with the Hook3 constructs followed by lysis with 50 mM Tris, pH 7.4, 150 mM NaCl, 5 mM TCEP, 1 mM PMSF, and a protease inhibitor cocktail (Roche; 1 tablet per 50 ml). The protein was then purified using either glutathione agarose 4B (USB) or Strep-Tactin Superflow Plus resin (QIAGEN). After extensive washing and elution with either 10 mM reduced glutathione at pH 7.4 (for glutathione agarose) or 3 mM desthiobiotin (for Strep-Tactin resin), the protein was gel filtered using a HiPrep 16/60 Superdex S-200 HR column (GE Healthcare) in 20 mM Tris, pH 7.4, 50 mM NaCl, and 2 mM TCEP.

Pull-downs

Clarified porcine brain lysate was used to test the binding of endogenous dynein–dynactin to Hook3 constructs and was prepared as previously described (McKenney et al., 2014). For each dynein–dynactin pull-down, 500 µl porcine brain lysate in buffer A (30 mM Hepes, pH 7.4, 50 mM potassium acetate, 2 mM magnesium acetate, 1 mM EGTA, and 10% glycerol) was combined with 60 µl of 50% Strep-Tactin Sepharose slurry (GE Healthcare), 0.1% NP-40, 5 mM DTT, and 1 mM PMSF. SfGFP-tagged Hook3 constructs were added at 200–400 nM to the brain lysate and resin and incubated for 1–2 h at 4°C. The resin was pelleted and washed five times in 500 µl buffer A including 0.1% NP-40 and 5 mM DTT. After the final wash, the resin was resuspended in 50 µl loading buffer, and an equal volume of the samples was resolved on NuPAGE gels (Invitrogen). All dynein–dynactin pull-downs were repeated at least three times on separate days starting from frozen brain lysate.

To test the binding of human LIC1 to Hook3 constructs, 200 nM GST-LIC1-strepII (full length or truncations) was incubated with 20 µl glutathione resin in a 300-µl volume of buffer (50 mM Tris, pH 7.4, 100 mM NaCl, 5 mM TCEP, 0.1% Tween, and 2 mg/ml BSA). After extensive washing of the resin, 300 µl of 200 nM sfGFP-Hook3 construct was added and incubated for 1 h at 4°C. The resin was washed extensively and resuspended in 20 µl of 1× loading buffer. Samples were resolved on NuPAGE gels. All pull-downs with purified LIC1 and Hook3 proteins were repeated at least three times on separate days.

Western blot analysis

After samples were resolved by SDS-PAGE, they were transferred to nitrocellulose membranes with the iBlot Gel Transfer Device (Invitrogen). Membranes were blocked with 5% milk in TBS and 0.1% Tween (TBST) and probed at RT with primary antibody, which included rabbit anti-GFP (1:1,000; Abcam), mouse anti-GST (1:1,000; Thermo Fisher Scientific), mouse anti-dynein intermediate chain (clone 74.1, 1:1,000; EMD Millipore), mouse anti-p150 (1:250; BD), and mouse anti-BicD2 (1:200; sc-393631; Santa Cruz Biotechnology, Inc.). Membranes were then washed three times with TBST and incubated with anti–mouse-800 or anti–rabbit-680 (1:10,000; Molecular Probes) for 45 min to 1 h at RT. Blots were visualized with an Odyssey Clx Infrared Imaging System (LI-COR Biosciences). Western blots were quantified using ImageJ (National Institutes of Health). A box was drawn around each band, and an equivalently sized box was drawn in the lane corresponding to the negative control. The intensity of each box was plotted, and the area under the subsequent curve was measured. The intensity of the negative control was subtracted from the corresponding sample. Band intensities of the prey in pull-downs were then normalized by the band intensities of the bait used in the assay (sfGFP-Hook3 or GST-LIC1). The prey's normalized intensities (arbitrary units) or the ratio of normalized intensities are presented. SDs were calculated for the intensities or ratio of intensities from three independent experiments and displayed as error bars. P values were calculated using an unpaired t test.

Crystallization and structure determination

The LIC1 C-terminal half (LIC$_{389–523}$) and GST-Hook3$_{1–160}$ were purified with glutathione agarose resin 4B (USB), cleaved from the resin using purified GST-tagged human rhinovirus 3C protease, and incubated overnight at 4°C. After the GST tag was cleaved, the two proteins were combined at an equimolar ratio and incubated on ice for 30 min. The proteins were gel filtered using a HiPrep 16/60 Superdex S-200 HR column (GE Healthcare) into the following buffer: 10 mM Tris, pH 7.4, 25 mM NaCl, and 2 mM TCEP. Fractions containing both proteins were concentrated to ~20 mg/ml, and hanging drop vapor diffusion experiments were set up using 96-well crystal screens (QIAGEN) at RT. Native crystals grew from a reservoir solution containing 2 M sodium formate and 0.1 M sodium acetate, pH 4.6 (JCSG screen Core III; QIAGEN). The crystals were cryoprotected with the addition of 35% glycerol to the crystallizing well solution and were flash cooled by plunging in liquid nitrogen.

Native diffraction data were collected at beamline 8.3.1 at the Advanced Light Source (Lawrence Berkeley National Laboratory), and the dataset was indexed and integrated in P 2 2$_1$ 2$_1$ using XDS (Kabsch, 2010). The structure was solved by molecular replacement using an ensemble of 20 superimposed NMR models from PDB structure 1WIX using Phaser (McCoy et al., 2007). The Phaser scores for the best solution were modest (RFZ = 4.8 and TFZ = 6.4), and the initial electron density maps were noisy and discontinuous. Density modification and chain tracing with SHELXE (Sheldrick, 2010) resulted in an easily interpretable map and a poly-alanine model that was further improved using phenix.autobuild (Terwilliger et al., 2008). Multiple rounds of model building and refinement were done using Coot (Emsley and Cowtan, 2004) and phenix.refine (Adams et al., 2010). The data collection and refinement states are presented in Table 1, and the PDB accession number is 5J8E.

Purification of dynein–dynactin from human RPE-1 cells

RPE-1 cell lysate was prepared as previously described (McKenney et al., 2014). The lysate was centrifuged at 266,000 g for 10 min at 4°C, and final concentrations of 5 mM DTT, 0.1% NP-40, and 1 mM PMSF were added before use. The lysate was incubated with purified strepII-SNAP-FIP3 on Strep-Tactin Sepharose (GE Healthcare). After incubation at 4°C for 1–2 h, the resin was thoroughly washed with buffer A (30 mM Hepes, pH 7.4, 50 mM potassium acetate, 2 mM magnesium acetate, 1 mM EGTA, 10% glycerol, 5 mM DTT, 0.1% NP-40, and 1 mM PMSF) and resuspended in buffer A with 300 mM NaCl to release dynein–dynactin from resin-bound FIP3. After incubating on ice for 10 min, the high-salt slurry was centrifuged through a 0.2-µm filter to remove the resin. Then an equal volume of 50% Strep-Tactin Sepharose slurry was added to the elution to bind any strepII-FIP3 that may have released from the resin during the high-salt incubation. After incubating on ice for 10 min, the slurry was once again filtered, and the final solution was diluted with buffer A for a final concentration of 200 mM NaCl. Sucrose was also added at a final 6% concentration, and the affinity-purified dynein–dynactin was flash frozen for single molecule imaging.

Single-molecule imaging

Preparation of microtubules. Tubulin was purified from porcine brain and labeled (fluorescently or with biotin) as previously described (Castoldi and Popov, 2003). To polymerize microtubules, unlabeled tubulin was combined with biotin-labeled tubulin and fluorescent tubulin (640 nm fluorescence) at a ratio of ~10:2:1, respectively, in BRB80 (80 mM Pipes, 1 mM EGTA, and 1 mM MgCl₂) and 5 mM GTP. After incubating for 10 min at 37°C, taxol was added at a final concentration of 20 µM. To remove unpolymerized tubulin, the microtubules were layered over a 25% sucrose cushion and centrifuged at 65,000 g for 5 min at 22°C.

Preparation of dynein–dynactin–Hook3 complexes. A 30-µl reaction consisting of 10 nM sfGFP-tagged Hook3 and 5 µl of ~0.15 mg/ml native dynein–dynactin purified from RPE-1 cells was incubated in 30 mM Hepes, pH 7.4, 50 mM potassium acetate, 2 mM magnesium acetate, 1 mM EGTA, 10% glycerol, 0.1 mg/ml BSA, 0.5% pluronic acid F-127, 0.2 mg/ml κ-casein, and a Trolox/PCA/PCD scavenging system (Dave et al., 2009).

TIRF microscopy. Flow chambers (volume ~10 µl) were constructed using double-sided tape and acid-washed coverslips as described (Tanenbaum et al., 2013). The chambers were prepared with immobilized fluorescent microtubules by coating the chamber in the following sequence of solutions: 10 µl of 5 mg/ml BSA-biotin (Thermo Fisher Scientific), 20 µl BC buffer (BRB80, 1 mg/ml BSA, 1 mg/ml casein, and 0.5% pluronic acid F-68, pH 6.8), 10 µl of 0.5 mg/ml streptavidin (Vector Laboratories), 20 µl BC buffer, and finally 10 µl of a 1:10 dilution of microtubules (prepared as described earlier). Microtubules were washed with the assay buffer, and a 1:10 dilution of the dynein–dynactin–Hook3 complex described earlier was added to the flow chamber in the presence of 1 mM ATP. Movies were acquired with an Eclipse TE200-E microscope (Nikon) equipped with an iXon EM CCD camera (Andor), a 100× 1.49-NA objective, and Micromanager software (Edelstein et al., 2010). A 491-nm laser (at 75% laser power) and a 640-nm laser (at half maximum laser power) were used to image sfGFP-Hook3 (100 ms exposure) and fluorescently labeled microtubules (50 ms exposure), respectively. Several 6-min movies (1- or 2-s intervals of image acquisition) were acquired at RT per flow chamber per construct. Molecules that moved >1 µm were scored as processive. Velocities were quantified by making kymographs in ImageJ (National Institutes of Health).

Online supplemental material

Fig. S1 shows the complete gels and relative inputs for pull-downs of Fig. 1, and it shows the co-gel filtration of LIC1₃₈₉₋₅₂₃ and Hook3₁₋₂₃₉. Fig. S2 shows the alignment of human Hook3 and mouse Hook1 (PDB 1WIX), and it displays the conservation of the Hook domains of the human Hook isoforms. Fig. S3 shows the sequence alignment used to map the conservation of Hook domains onto the Hook3₁₋₁₆₀ structure in Fig. 2 B. Fig. S4 presents the gel filtration chromatograms of all Hook3 proteins with triple mutations and full gels corresponding to Figs. 3 and 4. The purity of dynein–dynactin used in motility assays is also shown in Fig. S4. Fig. S5 displays the predicted coiled coils of Hook3, Hook3's interaction with microtubules in the presence and absence of dynein–dynactin, and additional data relevant to the motility assay in Fig. 5 (E and F). Online supplemental material is available at http://www.jcb.org/cgi/content/full/jcb.201604002/DC1.

References

Adams, P.D., P.V. Afonine, G. Bunkóczi, V.B. Chen, I.W. Davis, N. Echols, J.J. Headd, L.-W. Hung, G.J. Kapral, R.W. Grosse-Kunstleve, et al. 2010. PHENIX: A comprehensive Python-based system for macromolecular structure solution. *Acta Crystallogr. D Biol. Crystallogr.* 66:213–221. http://dx.doi.org/10.1107/S0907444909052925

Allan, V.J. 2011. Cytoplasmic dynein. *Biochem. Soc. Trans.* 39:1169–1178. http://dx.doi.org/10.1042/BST0391169

Bhabha, G., G.T. Johnson, C.M. Schroeder, and R.D. Vale. 2016. How dynein moves along microtubules. *Trends Biochem. Sci.* 41:94–105. http://dx.doi.org/10.1016/j.tibs.2015.11.004

Bielska, E., M. Schuster, Y. Roger, A. Berepiki, D.M. Soanes, N.J. Talbot, and G. Steinberg. 2014. Hook is an adapter that coordinates kinesin-3 and dynein cargo attachment on early endosomes. *J. Cell Biol.* 204:989–1007. http://dx.doi.org/10.1083/jcb.201309022

Brown, A.K., S.D. Hunt, and D.J. Stephens. 2014. Opposing microtubule motors control motility, morphology and cargo segregation during ER-to-Golgi transport. *Biol. Open.* 3:307–313. http://dx.doi.org/10.1242/bio.20147633

Carter, A.P., A.G. Diamant, and L. Urnavicius. 2016. How dynein and dynactin transport cargos: A structural perspective. *Curr. Opin. Struct. Biol.* 37:62–70. http://dx.doi.org/10.1016/j.sbi.2015.12.003

Castoldi, M., and A.V. Popov. 2003. Purification of brain tubulin through two cycles of polymerization-depolymerization in a high-molarity buffer. *Protein Expr. Purif.* 32:83–88. http://dx.doi.org/10.1016/S1046-5928(03)00218-3

Chowdhury, S., S.A. Ketcham, T.A. Schroer, and G.C. Lander. 2015. Structural organization of the dynein-dynactin complex bound to microtubules. *Nat. Struct. Mol. Biol.* 22:345–347. http://dx.doi.org/10.1038/nsmb.2996

Cianfrocco, M.A., M.E. DeSantis, A.E. Leschziner, and S.L. Reck-Peterson. 2015. Mechanism and regulation of cytoplasmic dynein. *Annu. Rev. Cell Dev. Biol.* 31:83–108. http://dx.doi.org/10.1146/annurev-cellbio-100814-125438

Dave, R., D.S. Terry, J.B. Munro, and S.C. Blanchard. 2009. Mitigating unwanted photophysical processes for improved single-molecule fluorescence imaging. *Biophys. J.* 96:2371–2381. http://dx.doi.org/10.1016/j.bpj.2008.11.061

Dienstbier, M., and X. Li. 2009. Bicaudal-D and its role in cargo sorting by microtubule-based motors. *Biochem. Soc. Trans.* 37:1066–1071. http://dx.doi.org/10.1042/BST0371066

Drozdetskiy, A., C. Cole, J. Procter, and G.J. Barton. 2015. JPred4: A protein secondary structure prediction server. *Nucleic Acids Res.* 43(W1):W389–W394. http://dx.doi.org/10.1093/nar/gkv332

Edelstein, A., N. Amodaj, K. Hoover, R. Vale, and N. Stuurman. 2010. Computer control of microscopes using µManager. *Curr Protoc Mol Biol* Chapter 14:Unit 14.20–14.20.17.

Emsley, P., and K. Cowtan. 2004. Coot: model-building tools for molecular graphics. *Acta Crystallogr. D Biol. Crystallogr.* 60:2126–2132. http://dx.doi.org/10.1107/S0907444904019158

Fu, M.M., and E.L.F. Holzbaur. 2014. Integrated regulation of motor-driven organelle transport by scaffolding proteins. *Trends Cell Biol.* 24:564–574. http://dx.doi.org/10.1016/j.tcb.2014.05.002

Harbury, P.B., T. Zhang, P.S. Kim, and T. Alber. 1993. A switch between two-, three-, and four-stranded coiled coils in GCN4 leucine zipper mutants. *Science.* 262:1401–1407. http://dx.doi.org/10.1126/science.8248779

Hoogenraad, C.C., A. Akhmanova, S.A. Howell, B.R. Dortland, C.I. De Zeeuw, R. Willemsen, P. Visser, F. Grosveld, and N. Galjart. 2001. Mammalian Golgi-associated Bicaudal-D2 functions in the dynein-dynactin pathway by interacting with these complexes. *EMBO J.* 20:4041–4054. http://dx.doi.org/10.1093/emboj/20.15.4041

Hoogenraad, C.C., P. Wulf, N. Schiefermeier, T. Stepanova, N. Galjart, J.V. Small, F. Grosveld, C.I. de Zeeuw, and A. Akhmanova. 2003. Bicaudal D induces selective dynein-mediated microtubule minus end-directed transport. *EMBO J.* 22:6004–6015. http://dx.doi.org/10.1093/emboj/cdg592

Horgan, C.P., S.R. Hanscom, R.S. Jolly, C.E. Futter, and M.W. McCaffrey. 2010. Rab11-FIP3 links the Rab11 GTPase and cytoplasmic dynein to mediate transport to the endosomal-recycling compartment. *J. Cell Sci.* 123:181–191. http://dx.doi.org/10.1242/jcs.052670

Hughes, S.M., K.T. Vaughan, J.S. Herskovits, and R.B. Vallee. 1995. Molecular analysis of a cytoplasmic dynein light intermediate chain reveals homology to a family of ATPases. *J. Cell Sci.* 108:17–24.

Kabsch, W. 2010. Xds. *Acta Crystallogr. D Biol. Crystallogr.* 66:125–132. http://dx.doi.org/10.1107/S0907444909047337

Kardon, J.R., S.L. Reck-Peterson, and R.D. Vale. 2009. Regulation of the processivity and intracellular localization of *Saccharomyces cerevisiae* dynein by dynactin. *Proc. Natl. Acad. Sci. USA.* 106:5669–5674. http://dx.doi.org/10.1073/pnas.0900976106

Kong, S., X. Du, C. Peng, Y. Wu, H. Li, X. Jin, L. Hou, K. Deng, T. Xu, and W. Tao. 2013. Dlic1 deficiency impairs ciliogenesis of photoreceptors by destabilizing dynein. *Cell Res.* 23:835–850. http://dx.doi.org/10.1038/cr.2013.59

Koushika, S.P., A.M. Schaefer, R. Vincent, J.H. Willis, B. Bowerman, and M.L. Nonet. 2004. Mutations in *Caenorhabditis elegans* cytoplasmic dynein components reveal specificity of neuronal retrograde cargo. *J. Neurosci.* 24:3907–3916. http://dx.doi.org/10.1523/JNEUROSCI.5039-03.2004

Krämer, H., and M. Phistry. 1999. Genetic analysis of hook, a gene required for endocytic trafficking in *Drosophila. Genetics.* 151:675–684.

Lupas, A., M. Van Dyke, and J. Stock. 1991. Predicting coiled coils from protein sequences. *Science.* 252:1162–1164. http://dx.doi.org/10.1126/science.252.5009.1162

Maldonado-Báez, L., N.B. Cole, H. Krämer, and J.G. Donaldson. 2013. Microtubule-dependent endosomal sorting of clathrin-independent cargo by Hook1. *J. Cell Biol.* 201:233–247. http://dx.doi.org/10.1083/jcb.201208172

Malone, C.J., L. Misner, N. Le Bot, M.C. Tsai, J.M. Campbell, J. Ahringer, and J.G. White. 2003. The *C. elegans* hook protein, ZYG-12, mediates the essential attachment between the centrosome and nucleus. *Cell.* 115:825–836. http://dx.doi.org/10.1016/S0092-8674(03)00985-1

McCoy, A.J., R.W. Grosse-Kunstleve, P.D. Adams, M.D. Winn, L.C. Storoni, and R.J. Read. 2007. Phaser crystallographic software. *J. Appl. Cryst.* 40:658–674. http://dx.doi.org/10.1107/S0021889807021206

McKenney, R.J., W. Huynh, M.E. Tanenbaum, G. Bhabha, and R.D. Vale. 2014. Activation of cytoplasmic dynein motility by dynactin-cargo adapter complexes. *Science.* 345:337–341. http://dx.doi.org/10.1126/science.1254198

McKenney, R.J., W. Huynh, R.D. Vale, and M. Sirajuddin. 2016. Tyrosination of α-tubulin controls the initiation of processive dynein-dynactin motility. *EMBO J.* 35:1175–1185. http://dx.doi.org/10.15252/embj.201593071

Moynihan, K.L., R. Pooley, P.M. Miller, I. Kaverina, and D.M. Bader. 2009. Murine CENP-F regulates centrosomal microtubule nucleation and interacts with Hook2 at the centrosome. *Mol. Biol. Cell.* 20:4790–4803. http://dx.doi.org/10.1091/mbc.E09-07-0560

Palmer, K.J., H. Hughes, and D.J. Stephens. 2009. Specificity of cytoplasmic dynein subunits in discrete membrane-trafficking steps. *Mol. Biol. Cell.* 20:2885–2899. http://dx.doi.org/10.1091/mbc.E08-12-1160

Pfister, K.K., and K.W.H. Lo. 2012. Cytoplasmic dynein function defined by subunit composition. *In* Dyneins. S.M. King, editor. Academic Press, London. 24–439. http://dx.doi.org/10.1016/B978-0-12-382004-4.10015-9

Pfister, K.K., P.R. Shah, H. Hummerich, A. Russ, J. Cotton, A.A. Annuar, S.M. King, and E.M.C. Fisher. 2006. Genetic analysis of the cytoplasmic dynein subunit families. *PLoS Genet.* 2:e1–e16. http://dx.doi.org/10.1371/journal.pgen.0020001

Sano, H., M. Ishino, H. Krämer, T. Shimizu, H. Mitsuzawa, C. Nishitani, and Y. Kuroki. 2007. The microtubule-binding protein Hook3 interacts with a cytoplasmic domain of scavenger receptor A. *J. Biol. Chem.* 282:7973–7981. http://dx.doi.org/10.1074/jbc.M611537200

Schlager, M.A., H.T. Hoang, L. Urnavicius, S.L. Bullock, and A.P. Carter. 2014. In vitro reconstitution of a highly processive recombinant human dynein complex. *EMBO J.* 33:1855–1868. http://dx.doi.org/10.15252/embj.201488792

Schmidt, H. 2015. Dynein motors: How AAA+ ring opening and closing coordinates microtubule binding and linker movement. *BioEssays.* 37:532–543. http://dx.doi.org/10.1002/bies.201400215

Schroeder, C.M., J.M.L. Ostrem, N.T. Hertz, and R.D. Vale. 2014. A Ras-like domain in the light intermediate chain bridges the dynein motor to a cargo-binding region. *eLife.* 3:e03351. http://dx.doi.org/10.7554/eLife.03351

Schroer, T.A. 2004. Dynactin. *Annu. Rev. Cell Dev. Biol.* 20:759–779. http://dx.doi.org/10.1146/annurev.cellbio.20.012103.094623

Sheldrick, G.M. 2010. Experimental phasing with SHELXC/D/E: Combining chain tracing with density modification. *Acta Crystallogr. D Biol. Crystallogr.* 66:479–485. http://dx.doi.org/10.1107/S0907444909038360

Szebenyi, G., B. Hall, R. Yu, A.I. Hashim, and H. Krämer. 2007. Hook2 localizes to the centrosome, binds directly to centriolin/CEP110 and contributes to centrosomal function. *Traffic.* 8:32–46. http://dx.doi.org/10.1111/j.1600-0854.2006.00511.x

Tan, S.C., J. Scherer, and R.B. Vallee. 2011. Recruitment of dynein to late endosomes and lysosomes through light intermediate chains. *Mol. Biol. Cell.* 22:467–477. http://dx.doi.org/10.1091/mbc.E10-02-0129

Tanenbaum, M.E., R.D. Vale, and R.J. McKenney. 2013. Cytoplasmic dynein crosslinks and slides anti-parallel microtubules using its two motor domains. *eLife.* 2:e00943. http://dx.doi.org/10.7554/eLife.00943

Terwilliger, T.C., R.W. Grosse-Kunstleve, P.V. Afonine, N.W. Moriarty, P.H. Zwart, L.-W. Hung, R.J. Read, and P.D. Adams. 2008. Iterative model building, structure refinement and density modification with the PHENIX AutoBuild wizard. *Acta Crystallogr. D Biol. Crystallogr.* 64:61–69. http://dx.doi.org/10.1107/S090744490705024X

Torisawa, T., M. Ichikawa, A. Furuta, K. Saito, K. Oiwa, H. Kojima, Y.Y. Toyoshima, and K. Furuta. 2014. Autoinhibition and cooperative activation mechanisms of cytoplasmic dynein. *Nat. Cell Biol.* 16:1118–1124. http://dx.doi.org/10.1038/ncb3048

Tripathy, S.K., S.J. Weil, C. Chen, P. Anand, R.B. Vallee, and S.P. Gross. 2014. Autoregulatory mechanism for dynactin control of processive and diffusive dynein transport. *Nat. Cell Biol.* 16:1192–1201. http://dx.doi.org/10.1038/ncb3063

Tynan, S.H., A. Purohit, S.J. Doxsey, and R.B. Vallee. 2000. Light intermediate chain 1 defines a functional subfraction of cytoplasmic dynein which binds to pericentrin. *J. Biol. Chem.* 275:32763–32768. http://dx.doi.org/10.1074/jbc.M001536200

Urnavicius, L., K. Zhang, A.G. Diamant, C. Motz, M.A. Schlager, M. Yu, N.A. Patel, C.V. Robinson, and A.P. Carter. 2015. The structure of the dynactin complex and its interaction with dynein. *Science.* 347:1441–1446. http://dx.doi.org/10.1126/science.aaa4080

Walenta, J.H., A.J. Didier, X. Liu, and H. Krämer. 2001. The Golgi-associated hook3 protein is a member of a novel family of microtubule-binding proteins. *J. Cell Biol.* 152:923–934. http://dx.doi.org/10.1083/jcb.152.5.923

Xu, L., M.E. Sowa, J. Chen, X. Li, S.P. Gygi, and J.W. Harper. 2008. An FTS/Hook/p107(FHIP) complex interacts with and promotes endosomal clustering by the homotypic vacuolar protein sorting complex. *Mol. Biol. Cell.* 19:5059–5071. http://dx.doi.org/10.1091/mbc.E08-05-0473

Yao, X., X. Wang, and X. Xiang. 2014. FHIP and FTS proteins are critical for dynein-mediated transport of early endosomes in *Aspergillus. Mol. Biol. Cell.* 25:2181–2189. http://dx.doi.org/10.1091/mbc.E14-04-0873

Zhang, J., R. Qiu, H.N. Arst Jr., M.A. Peñalva, and X. Xiang. 2014. HookA is a novel dynein-early endosome linker critical for cargo movement in vivo. *J. Cell Biol.* 204:1009–1026. http://dx.doi.org/10.1083/jcb.201308009